Arabian Journal of Geosciences (2021) 14: 2176
https://doi.org/10.1007/s12517-021-08483-4

3RD CAJG 2020

Radiological risk assessment of particulate matters in urban areas in Kuwait

Anfal Ismaeel[1] · Abdulaziz Aba[1] · Aishah Al-Boloushi[1] · Hanadi Al-Shammari[1] · Omar Al-Boloushi[1]

Received: 30 March 2021 / Accepted: 17 September 2021 / Published online: 19 October 2021

Abstract

Both natural and artificial radioactive airborne particles (RAPs) scatter over long distances and in a variety of directions. Vulnerability to the *RAPs* can result in an internal radiation exposure, which must be estimated, particularly in areas, such as Kuwait, where dust is prevalent. The aim of this study is to determine the radiation risks associated with inhaling various diameters of *RAPs*. Air samples were collected from various residential areas in Kuwait using high-volume air samplers with a five-stage cascade impactor. Radioactivity amounts of ^{7}Be, ^{40}K, ^{210}Pb, ^{210}Po, ^{137}Cs, and U isotopes were determined in three particle sizes (10.2, 2.4, and less than 0.73 μm). In addition, the daughter radionuclides of ^{222}Rn and ^{220}Rn, with comparatively small half-lives, were obtained and analyzed in particle sizes less than 10 μm. The abundance of all gamma and alpha emitters radionuclides in air samples was determined using low background gamma spectrometry systems and chemical separation methods of ^{210}Po and U isotopes.

Keywords Radioactive aerosols · Effective dose · ^{210}Po · ^{210}Pb · ^{7}Be

Introduction

Natural and artificial radionuclides can move long distances and scatter in various directions when released into the atmosphere. The chemical and physical properties of atmospheric aerosols affect the mobility of nuclear aerosols, also known as radioactive airborne particles (RAPs). Although natural origins of atmospheric radiation (cosmogonic radiation, ^{222}Rn and ^{220}Rn progeny, and resuspension of terrestrial radionuclides) have been present in the atmosphere since the Earth's formation, but artificial ionizing radiations (fission and activation radionuclides) have only been present since the testing of nuclear weapons in the middle of the last century (Papastefanou 2008). The internal effective dose that results from the inhalation of *RAP*s depends on the activity median aerodynamic diameter (AMAD), the type of radionuclide attached to the aerosol, and the amounts of radionuclides inhaled (Eckerman et al. 2012). Therefore, to estimate the internal effective dose, sufficient information on the types, sizes, and forms of radioactive airborne particles in the atmosphere is required. In addition, their radioactivity concentrations and their accumulation within the human body should also be determined.

Natural and anthropogenic compounds of various *AMAD*s are found in airborne particles. PM_{10}, or less than 10 μm AMAD, can interact with various respirable particles and cause adverse health effects on humans. As a result, Jancsek-Turóczi et al. (2013) lists it as one of the most harmful air pollutants for humans. Most experts and environmental regulatory agencies are now looking into the causes and health effects of fine and ultrafine airborne particles ($PM_{2.5}$ and $PM_{0.1}$, respectively) (Jancsek-Turóczi 2013; Balasubramanian 2004). In addition to cluster formation, some radionuclides interact rapidly with the current aerosols in the atmosphere, forming radioactive aerosols in a time ranging from 1 to 100 s (Fig. 1)(Papastefanou 2008). All radionuclides in the atmosphere are easily dissolved by solid particles in the atmosphere, and their activity is affected by both the chemical and the physical properties of the atmospheric aerosol.

Considerable studies were carried out in Kuwait addressing the adverse health effects associated with the

This paper was selected from the 3rd Conference of the Arabian Journal of Geosciences (CAJG), Tunisia 2020

Responsible Editor: Zhihua Zhang

✉ Anfal Ismaeel
aismaeel@KISR.edu.kw

[1] Environment and Life Sciences Research Center, Kuwait Institute for Scientific Research, P. O. Box 24885, 13109 Safat, Kuwait

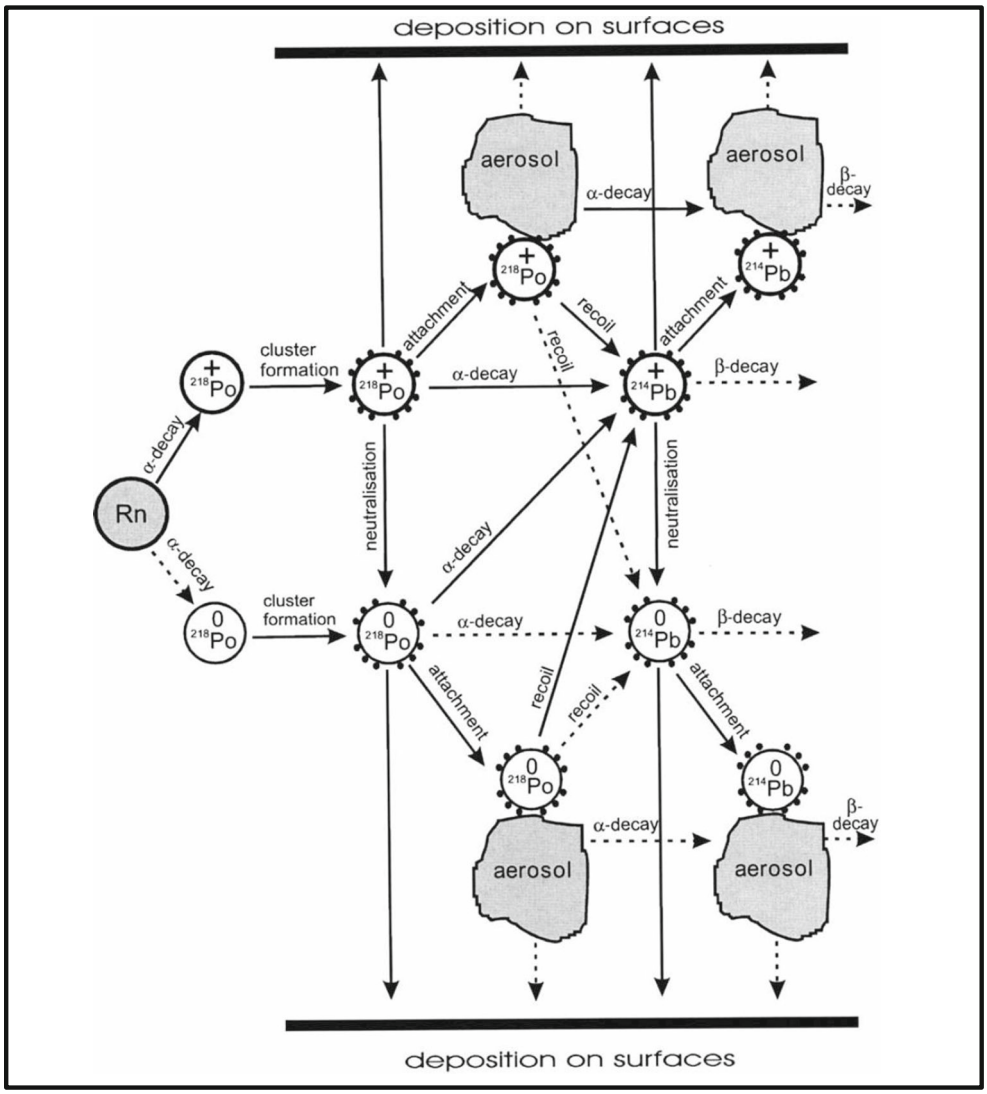

Fig. 1 Formation of radioactive aerosol due to Radon-222 (Papastefanou 2008).

high concentration of $PM_{2.5}$ and PM_{10}. It has been found that sand dust, oil burning, the petrochemical industry, traffic, and anthropogenic sources from outside Kuwait are the primary sources of $PM_{2.5}$ (Aba et al. 2020; Al-Hemoud et al. 2019; Alolayan et al. 2013). Alolayan et al. (2013) observed that sand dust was responsible for around 54% of $PM_{2.5}$ particles, and the average annual $PM_{2.5}$ level in Kuwait is 53 $\mu g/m^3$, which is five times higher than the World Health Organization (WHO) recommendations (10 $\mu g/m^3$).

Consequently, large data on radionuclide concentrations in atmospheric fallout are available worldwide (Aba et al. 2016, 2018, 2020; UNSCEAR 2020; Masson et al. 2019; Steinhauser 2018; Baeza et al. 2017; Sayed et al. 2002). Several experiments on ^{7}Be, ^{137}Cs, ^{210}Po, and ^{210}Pb concentrations in the air have been conducted in Kuwait.

Moreover, many studies were focused on *AMAD*, to quantify the internal radiation exposures and the associated risk (Ismaeel et al. 2020; Ioannidou and Paatero 2014; Cho et al. 2007). Al-Azmi et al. (2001) analyzed the concentration of ^{7}Be in the atmosphere for five years, that is, from 1994 to 1998, and the average ^{7}Be concentration was estimated to be 5.2 mBq/m^3. Over the same time cycle, Sayed et al. (2002) used a liquid scintillation counter to calculate the concentration of ^{210}Pb in the atmosphere and analyze the sum and concentration in air filters. From 2009 to 2011, Aba et al. (2016) studied the ranges of radioactivity in dust in Kuwait. ^{210}Pb, ^{7}Be, and ^{137}Cs radionuclides had annual average depositional fluxes of around 134, 422, and 4.3 Bq/m^2, respectively. The effects of radionuclide deposition were found to be highly correlated with dust deposition (Aba et al. 2016; Al-Dousari et al. 2016).

This study estimated the radiological risk associated with inhaled *RAP*s of different *AMAD*s in pre-selected residential areas in Kuwait. The results could be used by the public authorities in the country for better environmental management and public health awareness. The generated data will be used as a radioactive airborne exposure baseline within the national air quality monitoring program.

Methods

Sampling and sample preparation

High-volume air samplers (HVAS) compatible with a five-stage cascade impactor were used to gather air filters from five residential areas in Kuwait (Fig. 2). During the sampling time (3 d), the flow rates were set to 420 l/min to collect a sample volume of 1700 m^3; the samples were assembled every week. The quartz microfiber filter (MFQ), 150×143 mm, and *MFQ* 203× 254 mm, were used for sampling (Staplex Co. Inc).

The air filters were divided into the following three categories based on the fraction sizes of aerosols:

- Seq 6, with particle sizes smaller than 0.73 μm,
- Seq 4–5, with fraction sizes from 0.73 to 2.4 μm, and
- Seq 1–3, with fraction sizes from 2.4 to 10.2 μm.

This procedure was designed to minimize the measurement time and maximize the sample volume to meet lower detection limits in less time. Unlike the sampling process for long half-life radionuclides, the sampling method for short half-lives of radon and thoron progenies, namely, ^{214}Bi ($T_{½}$ = 60.6 min), ^{212}Pb ($T_{½}$ = 10.6 h), and ^{214}Pb ($T_{½}$ = 26.8 min), involved 3 h of filtration using an *MFQ* filter with a scale of 203×254 mm. In addition, the interval between sampling and counting (waiting time) did not exceed 1 h. This experiment was carried out once a week at the Kuwait Institute for Scientific Research (KISR) (Shuwaikh location), which is adjacent to the Radiation Measurements Laboratory (RML), and the measurement was completed in less than one hour.

Radioactivity measurements

Two gamma spectrometry systems, i.e., Ultralow Background (ULB) Detector System and N-type Canberra systems (Canberra Inc.), were used to measure the activity concentration of ^{7}Be, ^{40}K, ^{210}Pb, ^{137}Cs, ^{212}Pb,

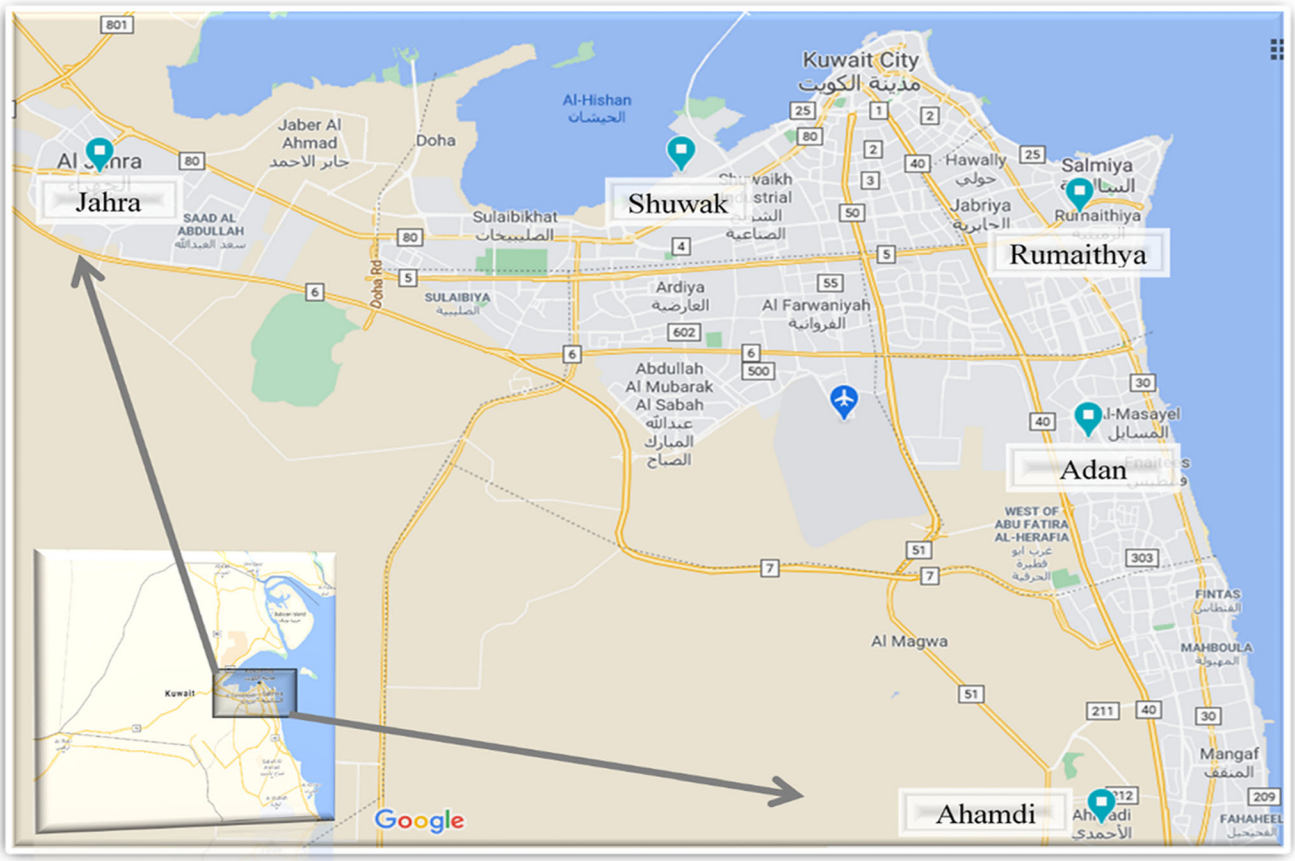

Fig. 2 Sampling locations.

^{214}Pb, and ^{214}Bi radionuclides, whereas chemical separation methods and alpha spectroscopy were used to measure the activity concentrations of ^{210}Po, ^{238}U, and ^{234}U. Both gamma spectrometry systems were equipped with high-purity germanium (HPGe) detectors with specifications fulfilled to determine low and high gamma energy concentrations. The *ULB* gamma spectrometry system was fitted with broad energy germanium (BEGe) detector type, which had a surface area of 5000 mm^2 with good efficiency for low gamma energy (FWHM at122 keV is 750 eV). It was shielded with ultralow background materials (lead and copper) and supported with Veto shielding to reduce the cosmic ray interferences. The second system was equipped with a reverse electrode germanium (REGe) detector type of 100% relative efficiency and shielded with low background lead.

Gamma analytical software (Genie-2000) developed by Canberra was used for gamma spectra analyses. The nuclear library used by this software was updated using online data from Laboratories National Henri Becquerel, France. A compatible simulation software, LabSOCS (Canberra Inc.), was used to generate an efficiency calibration curve for each detector that appropriated with the normalized air filters' geometry. The calibration curves were used to calculate the activity concentrations of different gamma emitter radionuclides.

A formula was elaborated for activity calculation of radionuclides taking into account the accumulation and decay correction factor during filtration, preparation, and counting as follows:

$$\mathrm{Ao} = \frac{\sum(area).(\lambda_i)^2.e^{+\lambda_i t_d}}{(1-.e^{-\lambda_i t_c}).(1-.e^{-\lambda_i t_f}).v.I_{\gamma i}.\epsilon_{di}} \quad (1)$$

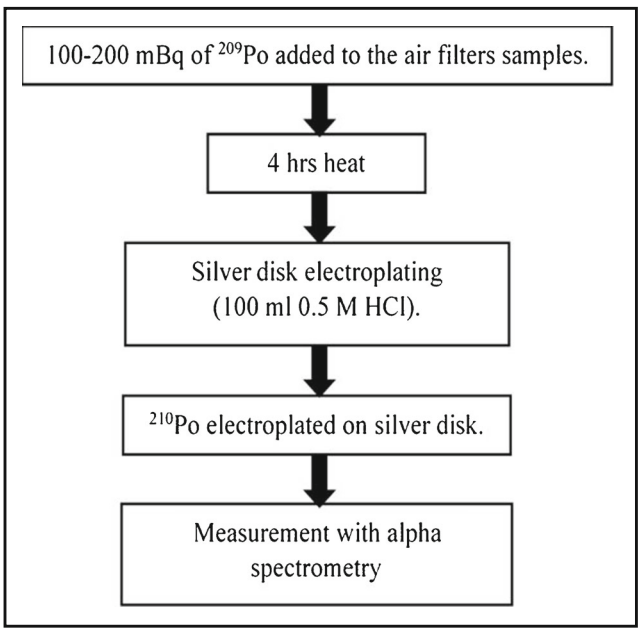

Fig. 3 Procedure followed for the Po analysis.

where A_o is the concentration of activity particular radionuclide in air (Bq/m^3); V is flow rate (m^3/s); I_γ is ɣ-ray emission rate; ε_d is detection efficiency; λ_i is the decay constant of nuclide of interest; and t_d, t_c, and t_f are the delay, counting, and filtering times, respectively.

To test the alpha emitters radionuclides Po and U isotopes, air filters were separated into two halves. Each radionuclide was analyzed using one-half of the sample. Radiochemistry protocols for ^{210}Po and U isotopes were used to isolate the alpha emitters radionuclides in air filters. The ^{210}Po was measured using a rapid chemical leaching process (Fig. 3). Every month, the air filter samples were combined into one sample for the measurement of uranium radioisotopes as the concentration of U in the filters was low. The radiochemistry technique employed for uranium radioisotopes' research is seen in Fig. 4 (Alboloushi et al. 2020). Measurements were taken for a minimum of 2 days using Canberra alpha spectrometer.

Quality control

An internal calibration source was prepared in the *RML* laboratory using a known concentration of a certified reference solution of mixed gamma radionuclides (QCYB40 and QCYB41 from Isotrak, Germany), applied to a blank filter with the same geometry as the air filter samples used in this analysis. This calibration source was used to verified the detector' efficiency calibration curves produced by LabSOCS software. In addition, to estimate the chemical recovery and check the detector's accuracy, each batch of air filters was analyzed alongside the certified reference material. The accuracy of the alpha spectrometry system was also validated using an accredited reference standard from Eckert and Ziegler (NK 225).

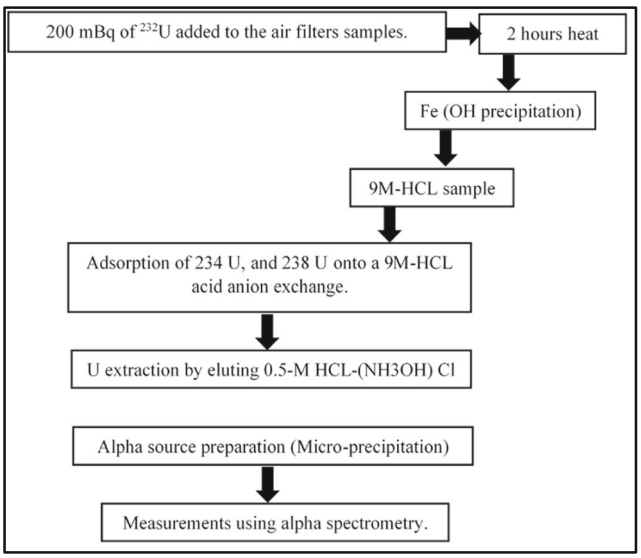

Fig. 4 Procedure followed for the U isotopes' analysis.

Internal effective dose and radiation risk assessment

Two methods were implemented to calculate the inhalation doses based on the short-lived radionuclides (radon and thoron progenies) and the long-lived radionuclides deposited on the filter (^{210}Po, ^{210}Pb, ^{7}Be, ^{40}K, and ^{137}Cs). In the first method, it was assumed that the ^{222}Rn progenies were almost equally produced during the decay. As a result, the adsorption processes of ^{218}Po and ^{214}Pb on the surface dust samples were very similar, and the other remaining radionuclides (^{214}Bi and ^{214}Po) were transiently radioactive in equilibrium with ^{214}Pb. The effective doses (EDs) from the outdoor inhalation of short-lived^{222}Rn daughters (ED_{Rn}) were estimated using Equation 2, taking into consideration the United Nations Scientific Committee on the Effects of Atomic Radiation (UNSCEAR) reported parameters.

$$\mathrm{ED_{Rn}[mSv/y]} = C \times A_{214_{Pb}} \times T_{ex} \quad (2)$$

where $A_{214_{Pb}}$ is an average outdoor concentration of ^{214}Pb in Bq·m^{-3} and T_{ex} is the outdoor occupancy time, usually 2000 h. The constant C equals 26.67×10^{-6}, which was derived from the adopted UNSCEAR 2019 report parameters of dose coefficient factor (DCF) (16×10^{-6} mSv per Bq. h. m^{-3}) divided by the adopted outdoor radon equilibrium factor (F) (0.6) (UNSCEAR 2020).

Similarly, the *ED* from the inhalation of thoron progeny (^{212}Pb) and its decay products (ED_{Th}) were estimated using the adopted UNSCEAR 2019 parameters of the *DCF,* which is 40×10^{-6} mSv per Bq. h. m^{-3}(Equation 3).

$$\mathrm{ED_{Th}[mSv/y]} = 40 \times 10^{-6} \times A_{212_{Pb}} \times T_{ex} \quad (3)$$

where $A_{212_{Pb}}$ is the average outdoor concentration of ^{212}Pb in Bq·m^{-3} and T_{ex} is the outdoor occupancy time, usually 2000 h.

In the same context, Equation 4 was applied to estimate the *ED*s for the residual radionuclides, which takes into account the *AMAD* of the inhaled particles, as well as the activity concentrations of each radionuclide. The *DCF* values of different *AMAD*s (1 and 5 μm) were adopted from International Commission on Radiological Protection (ICRP) 119 (Eckerman et al. 2017), where 5 μm was used for the composite samples of seq 1–3 and 1 μm was used for the composite samples of seq 4–5 and seq 6.

The annual *EDs* for various age groups were also calculated using age-specific*DCF* for the inhalation of the radionuclides tested (Equation 4).

$$ED_i = Ai.DCF_i.BRT.T_{ex}. \quad (4)$$

where *ED* is the effective dose (Sv) for the radionuclide i, *A* is the radioactivity concentration of the radionuclide i (Bq/m^3), *DCF* is the dose conversion factor (Sv/Bq) of the radionuclide i, *BRT* is the average daily breathing rate (m^3/h) (Brudecki et al. 2017), and T_{ex} is the estimated outdoor exposure time (h).

Finally, the minimum and maximum *ED*s were used to calculate the excess of lifetime cancer risk (ELCR) by applying Equation 5.

$$ELCR = E.DL.RF \quad (5)$$

where *DL* is the average duration of life, which is 70 years, and *RF* is the risk factor, 5. ×10^{-2} Sv^{-1} (ICRP 103)

Results and discussion

Radioactivity concentrations on aerosols

Table 1 shows the ranges of the radionuclides concentrated on atmospheric particulates of the total fractions (less than 10.2 μm) for 1-year measurements, which was calculated based on the geometric mean (GM) values and the geometric standard deviations (Motulsky 2021) of various areas. ^{7}Be activity concentrations varied over time in all stations, with the highest values observed in Kuwait during the summer months (July and August) (Ismaeel et al. 2020). During the hot weather, the normal convection of the air masses allows the falling of cool air masses filled from the troposphere and stratosphere, resulting in this difference (Persson and Holm 2014; Pham et al. 2011). The concentration findings of ^{40}K, on the other hand, showed no temporal fluctuations and no major deviations between the different sites (Ismaeel et al. 2020). However, the Jahra station had the highest activity concentration of ^{40}K because this site is a vast open area that enhances

Table 1 The ranges of the radionuclides concentrated on atmospheric particulates of the total fractions (GM) in mBq/m^3 in different stations

Location		*Area*	*^{40}K*	*^{7}Be*	*^{210}Pb*	*^{210}Po*
N	*E*					
29° 05′ 10″	48° 03′ 54″	Ahamdi	1.76–3.44 (2.46)	4.68–10.82 (7.12)	0.76–1.50 (1.07)	0.52–1.7 (0.96)
29° 20′ 22″	47° 54′ 21″	Shuwakh	1.45–2.68 (1.97)	4.17–10.28 (6.55)	0.60–1.37 (0.91)	0.24–1.07 (0.51)
29° 19′ 15″	48° 03′ 53″	Rumaithya	1.66–3.12 (2.28)	5.03–11.48 (7.60)	0.85–1.59 (1.16)	0.28–1.41 (0.63)
29° 20′ 27″	47° 41′ 45″	Jahra	1.80–3.58 (2.54)	4.28–10.55 (6.72)	0.69–1.49 (1.01)	0.34–0.83 (0.53)
29° 94′ 43″	48° 04′ 19″	Adan	1.85–3.48 (2.54)	3.93–9.69 (6.17)	0.71–1.40 (1.00)	0.34–2.11(0.85)

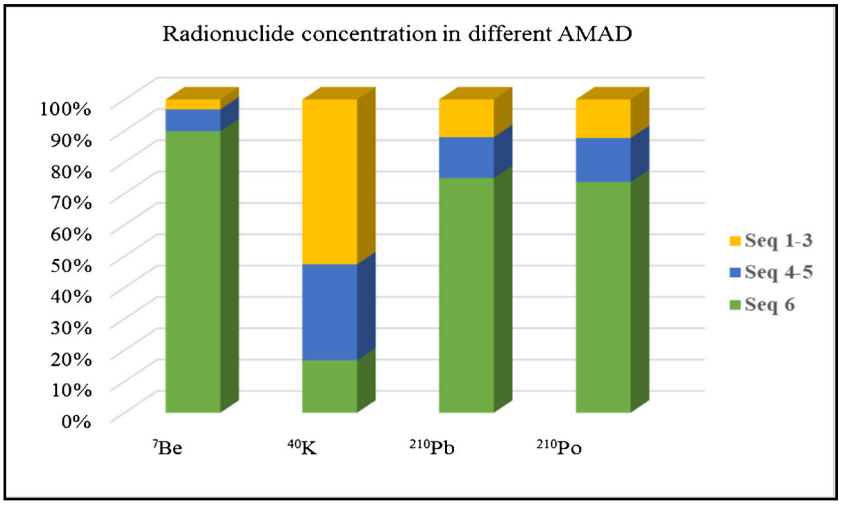

Fig. 5 Percentage of contribution of AMAD in each radionuclide concentration.

the generation of local dust storms, which are the primary sources of ^{40}K. The radioactivity concentrations of ^{210}Po were reported taking into account the ingrowth of natural ^{210}Po during the sample preparation. The results showed that both Ahmadi and Adan sites were an order of magnitude higher than the other sites as these areas are located close to the industrial areas (oil production and petrochemicals), which result in excessive concentrations of ^{210}Po (Aba et al. 2020; Persson and Holm 2014, Jonkers 1997). On the other hand, the concentrations of ^{210}Pb were almost within the same range in all stations. The ratio between ^{210}Po and ^{210}Pb is 0.86, which might indicate the impact of anthropogenic sources of ^{210}Po (Ismaeel et al. 2020).

Moreover, the relationship between the radionuclides' concentrations and different *AMAD*s is presented in Fig. 5. More than 70% of the radioactivity concentrations accumulated on the smallest fraction sizes (seq 6), except for ^{40}K, where 60% accumulated on particle sizes larger than 2.4 μm (seq 1–3) (Fig. 5). This may be due to the local origin of ^{40}K, where the dust resuspensions generated by the local dust storms enhance the aggregation of the smaller particle size fractions (Ismaeel et al. 2020). For all collected samples, both ^{238}U and ^{234}U values were below the concentration limits (1.96 and 1.91 μBq/m^3, respectively).

The total activity concentration of all short-lived radionuclides shows that the three radionuclides have the same trend (Fig. 6). The correlation coefficient between the total activities

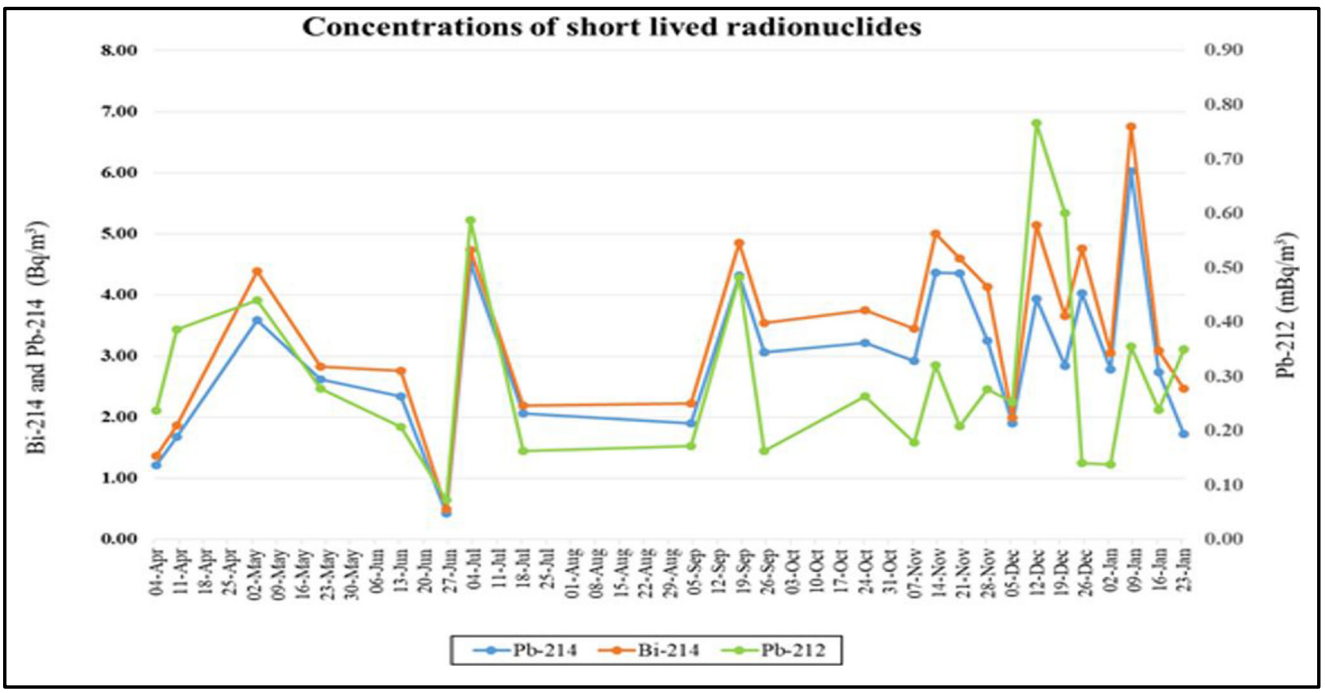

Fig. 6 Concentration of short-lived radionuclides

Table 2 Range of the effective dose from the inhalation of radionuclides in all stations (nSv/year)

Radionuclides	*Particles< 0.7 μm*	*Particles: 0.7–2.4 μm*	*Particles 2.4–10.2 μm*
^{7}Be	0.22–1.31	0.011–0.13	0.004–0.05
^{40}K	0.50–3.70	2.09–6.04	5.06–14.51
^{137}CS	0.05–0.12		0.06–0.14
^{210}Pb	435–2804	118–664	90–584
^{210}Po	94–11383	279–3210	239–1439
Total (μSv/y)	0.53–14.19	0.4–3.88	0.33–2.04

of ^{214}Pb and ^{212}Pb radionuclides is insignificant (R2; 0.18), representing different origins and behavior of ^{220}Rn and ^{222}Rn radionuclides in the surface air.

Dose estimations

The geometric mean of the radioactivity concentrations in all stations was used to calculate the cumulative internal effective doses through inhalation. Table 2 shows the ranges of the internal effective dose levels for different particle sizes. The findings revealed that the alpha emitter radionuclides ^{210}Po had the greatest impact on the annual effective dose. The *EDs* of the different fraction sizes were estimated based on the geometric mean of the radioactivity concentrations. The estimated annual *EDs* on seq 6, seq 4–5, and seq 1–3, were 3.85, 0.82, and 0.70 μSv, respectively. The calculation also showed that there were no significant differences in the total effective annual dose from different particle sizes of other geographical areas. However, the fraction sizes of seq 4–5 showed a slightly higher concentration values in Jahra (around 19%) than in the other areas (about 15%).

The age specific effective dose due to the inhalation of the long-lived radionuclide concentrations is presented in Fig. 7. The Geometry mean of radioactive concentration in the small fraction sizes, which is inhaled and reaches the pulmonary alveoli (less than 1 mm), was used to calculate the inhalation dose (Equation 4). The outdoor exposure period used in Equation 4 was estimated based on the Kuwaiti population's lifestyle, in which most of the outdoor occupancy factors were smaller than those of the other regions due to the hot weather. As a result, the time exposures for various ages ranged from 2000 h for adults to 356 h for infants. ^{210}Pb and ^{210}Po, as predicted, make a significant contribution to the annual inhalation effective dose because of the high *DCF* of both radionuclides (Table 2).

The contributions of the short-lived radionuclides (^{222}Rn and ^{220}Rn progenies) were estimated based on the total accumulated aerosols (less than 10.2 μm fraction) in Shuwaikh site only (Fig. 8). The obtained overall annual effective dose was about 95 μSv, which was significantly less than the total annual dose adopted for the general population in Kuwait (1 mSv/year). As expected, the contribution of ^{222}Rn was responsible for 93% (88.0 μSv/year) of the overall annual effective dose compared with 3% contribution (2.11 μSv/year) of ^{220}Rn. Finally, the excess *ELCR* range was estimated based on low and high radiation exposures in the Shuwaikh area, and it

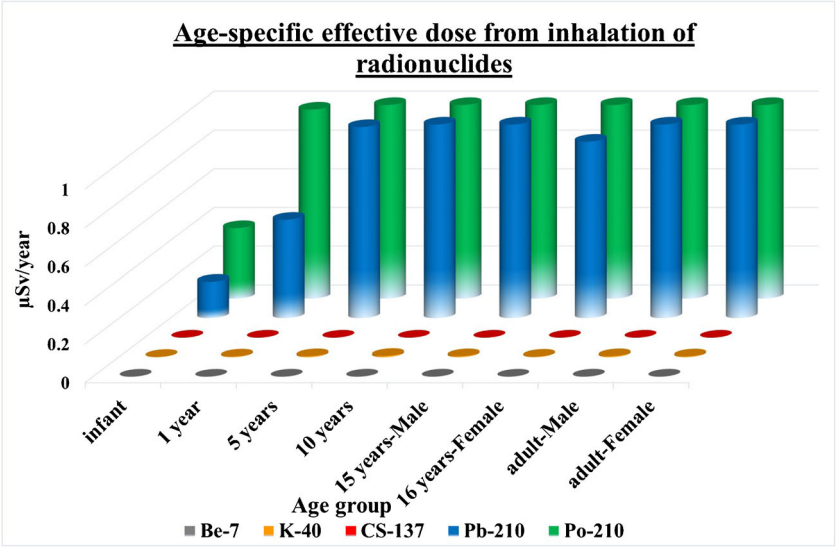

Fig. 7 Age specific effective dose due to inhalation.

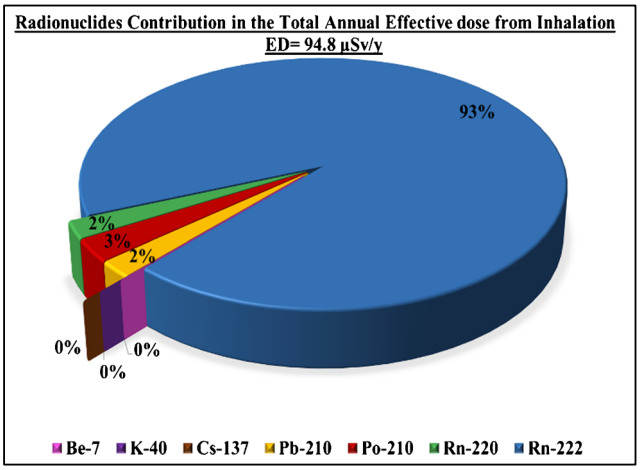

Fig. 8 Total effective annual dose from inhalation in Shuwaikh.

varied from 6.27×10^{-5} to 8.47×10^{-4} with a geometric mean of 3.65×10^{-4}. However, Al-Hemoud et al. (2019) reported the associations between high concentrations of $PM_{2.5}$ and high excess mortalities from different diseases (ischemic heart diseases, stroke, and respiratory diseases); the average was 393 cases per year per a 100,000 inhabitants in Kuwait. This figure is much higher the number of the excess cases due to the outdoor radiation exposures (36).

Conclusions

The study on the concentrations of radionuclides in the urban areas of Kuwait showed no significant difference between the studied residential areas, except for ^{210}Po, which was linked to the anthropogenic sources. On the other hand, the radionuclide concentrations of different *AMAD*s were considered significant according to their origin and deposition mechanism. The estimated annual internal effective dose due to inhalation can be negligible compared with the total radiation exposure limit for the public in Kuwait. The estimated *ELCR* due to the inhaled radiation dose was smaller than the excess lung cancer cases due to $PM_{2.5}$ exposures.

Author contribution All authors contributed to the study conception and design. Material preparation, data collection, and analysis were performed by Anfal Ismaeel, Abdulaziz Aba, Aishah Al-Boloushi, Hanadi Al-Shammari, and Omar Al-Boloushi. The first draft of the manuscript was written by Anfal Ismaeel and the comments of all authors on the various versions of the manuscript were taken into account. The final manuscript was read and approved by all authors.

Funding The Kuwait Foundation for the Advancement of Sciences (KFAS) had a major role in funding and supporting this project (Project Code P215-44WE-02, 2019).

Declarations

Competing interests The authors declare no competing interests.

References

Aba A, Ismaeel A, Al-Boloushi O, Al-Shammari H, Al-Boloushi A, Malak M (2020) Atmospheric residence times and excess of unsupported ^{210}Po in aerosol samples from the Kuwait bay-northern gulf. Chemosphere 261:127690

Aba A, Al-Dousari A, Ismaeel A (2018) Atmospheric deposition fluxes of ^{137}Cs associated with dust fallout in the northeastern Arabian Gulf. J Environ Radioact 192:565–572

Aba A, Al-Dousari A, Ismaeel A (2016) Depositional characteristics of ^{7}Be and ^{210}Pb in Kuwaiti dust. J Radioanal Nucl Chem 307(1):15–23

Al-Azmi D, Sayed AM, Yatim HA (2001) Variations in ^{7}Be concentrations in the atmosphere of Kuwait during the period 1994 to 1998. Appl Radiat Isot 55(3):413–417

Alboloushi A, Aba A, Alboloushi O, Ismaeel A, Al-Shammari H, Al-Jarba M (2020) Radioactive uranium and cesium levels in Kuwait Bay seawater. Arab J Geosci 13(6):1–8

Al-Dousari A, Aba A, Al-Awadhi S, Ahmed M, Al-Dousari N (2016) Temporal and spatial assessment of pollen, radionuclides, minerals and trace elements in deposited dust within Kuwait. Arab J Geosci 9(2):95

Al-Hemoud A, Gasana J, Al-Dabbous A, Alajeel A, Al-Shatti A, Behbehani W, Malak M (2019) Exposure levels of air pollution ($PM_{2.5}$) and associated health risk in Kuwait. Environ Res 179: 108730

Alolayan MA, Brown KW, Evans JS, Bouhamra WS, Koutrakis P (2013) Source apportionment of fine particles in Kuwait City. Sci Total Environ 448:14–25

Baeza A, Corbacho JA, Caballero JM, Ontalba MA, Vasco J, Valencia D (2017) Development of an advanced radioactive airborne particle monitoring system for use in early warning networks. J Radiol Prot 37(3):642–658

Balasubramanian, R., Qian W. B (2004) Characterization and source identification of airborne trace metals in Singapore. J Environ Monit 6.10: 813-818.

Brudecki K., Szufa K., Mietelski J. W (2017)^{131}I age-dependent inhalation dose in Southern Poland from Fukushima accident. Radiat Environ Biophys 56(1), 9-17.

Cho YH, Lee W, Chung KH, Choi GS, Lee CW (2007) Seasonal variation and activity size distribution of ^{7}Be in ambient air. J Radioanal Nucl Chem 274(3):531–538. https://doi.org/10.1007/s11356-020-09367-y

Eckerman K, Harrison J, Menzel HG, Clement CH (2017) ICRP publication 119: compendium of dose coefficients based on ICRP publication 60. Ann ICRP 42(4):e1–e130

Eckerman K, Harrison J, Menzel HG, Clement CH (2012) ICRP publication 119: Compendium of dose coefficients based on ICRP publication 60. Ann ICRP 41:1–130

Ioannidou A, Paatero J (2014) Activity size distribution and residence time of ^{7}Be aerosols in the Arctic atmosphere. Atmos Environ 88: 99–106

Ismaeel A, Aba A, Al-Shammari H, Al-Boloushi A, Al-Boloushi O, Malak M, Al-Dabbous A, Al-Tamimi S (2020) Activity size distributions of radioactive airborne particles in an arid environment: a case study of Kuwait. Environ Sci Pollut Res (26):33032–33041

Jancsek-Turóczi B, Hoffer A, Nyírő-Kósa GA (2013) Sampling and characterization of resuspended and respirable road dust. J Aerosol Sci 65:69–76

Jonkers G(1997) Characterization of NORM in the oil and gas production industry. Proc.of NORM.

Masson O., Steinhauser G., Zok D., Saunier O., Angelov H., Babić D., Bečková V., Bieringer J., Bruggeman M., Burbidge C.I, Conil, S (2019) Airborne concentrations and chemical considerations of radioactive ruthenium from an undeclared major nuclear release in

2017. Proc Natl Acad Sci, 116(34), pp:16750-16759. https://doi.org/10.1073/pnas.1907571116

Motulsky H. J. (2021) The geometric mean and geometric SD factor. GraphPad Statistics Guide. http://www.graphpad.com/guides/prism/latest/statistics/stat_the_geometric_mean_and_geometr.htm. Accessed 12 August 2021

Papastefanou C (2008) Radioactive aerosols. Radioact Environ 12:11–58

Persson BR, Holm E (2014) ^{7}Be, ^{210}Pb, and ^{210}Po in the surface air from the Arctic to Antarctica. J Environ Radioact 138:364–374

Pham MK, Betti M, Nies H, Povinec PP (2011) Temporal changes of ^{7}Be, 137Cs and ^{210}Pb activity concentrations in surface air at Monaco and their correlation with meteorological parameters. J Environ Radioact. 1;102(11):1045-54.

Sayed AM, Al-Azmi D, Khuraibet NA (2002) Measurements of ^{210}Pb concentrations in airborne in Kuwait. Environ Monit Assess 79(1): 47–55

Steinhauser G (2018) Anthropogenic radioactive particles in the environment. J Radioanal Nucl Chem 318(3):1629–1639

United Nations Scientific Committee on the Effects of Atomic Radiation (UNSCEAR) (2020) UNSCEAR 2019 Report to the General Assembly: Sources, Effects And Risks of Ionizing Radiation. United Nations: New York, NY